International Journal of Plasticity 61 (2014) 17–31

Contents lists available at ScienceDirect

International Journal of Plasticity

journal homepage: www.elsevier.com/locate/ijplas

# Martensite modulus dilemma in monoclinic NiTi-theory and experiments

J. Wang, H. Sehitoglu *

*Department of Mechanical Science and Engineering, University of Illinois at Urbana-Champaign, 1206 W. Green St., Urbana, IL 61801, USA*

ARTICLE INFO

*Article history:*
Received 26 February 2014
Received in final revised form 30 April 2014
Available online 4 June 2014

*Keywords:*
A. Twinning
A. Phase transformation
A. Dislocations
C. Mechanical testing
Elastic moduli

ABSTRACT

Correct assessment of the NiTi martensite moduli and its significance are the subject of this paper. Current experiments and published experimental data reveal the considerable difference between the macroscopic elastic moduli for twinned martensite and detwinned martensite (single crystal state). Although this difference is significant, it is not explained adequately, and often neglected in modeling. In this study, based on the atomistic simulations, we establish Voigt and Reuss bounds and Hill's estimate for macroscopic moduli for both the internally twinned states and single crystal (detwinned) states. The predicted elastic moduli in the twinned state compare favorably to the experimental thermally induced martensite (with internal twin arrangement) moduli. The single crystal moduli predictions conform to the experimental moduli for deformed martensite or stress-induced martensite in tension and compression showing asymmetry. We draw attention to the need for correct interpretation of the elastic moduli for understanding a wide range of phenomena in shape memory alloys, such as the transformation stress–strain response, the fatigue behavior, the stored elastic energy, the stress hysteresis and others.



## 1. Introduction

Due to the technological significance of NiTi shape memory alloys (SMAs) (Funakubo, 1987; Otsuka and Wayman, 1998), the knowledge of the elastic moduli of NiTi martensite is essential (Liu and Xiang, 1998; Sehitoglu et al., 2002), yet not well understood. The SMA's thermoelastic martensitic transformation depends on the stored elastic energy Ezaz et al., 2011; Wagner and Windl, 2008), which is a function of martensite elastic moduli. The mechanical response of SMAs, especially in the martensitic state, is rather complex because the martensite morphology undergoes a transition from a multi-variant ('internally twinned') state to a single variant (''detwinned'') arrangement (Liu et al., 1999; Sehitoglu et al., 2003). As transition occurs from a multi-variant twinned morphology to a single crystal one, the accompanying elastic moduli increase can be nearly a factor of three (from 50 GPa to 130 GPa in tension in NiTi). Furthermore, the martensite in binary NiTi has a monoclinic crystal structure with 13 constants (Hatcher et al., 2009; Wagner and Windl, 2008). Thus, phenomenological modeling efforts utilizing lower number of constants (ignoring the anisotropy) or same modulus for martensite relative to austenite may not conform to experiments (Auricchio et al., 1997; Liang and Rogers, 1990; Tanaka, 1986). Overall, there is an incomplete understanding of the elastic modulus in martensitic SMAs (Lagoudas, 2010). This is borne out by recent experimental efforts (Benafan et al., 2012; Šittner et al., 2013; Rajagopalan et al., 2005; Stebner et al., 2013) that have vigorously interrogated the 'overall' elastic moduli in NiTi utilizing various techniques, including high energy diffraction.

* Corresponding author. Tel.: +1 2173334112.
*E-mail address:* huseyin@illinois.edu (H. Sehitoglu).

http://dx.doi.org/10.1016/j.ijplas.2014.05.005
0749-6419/

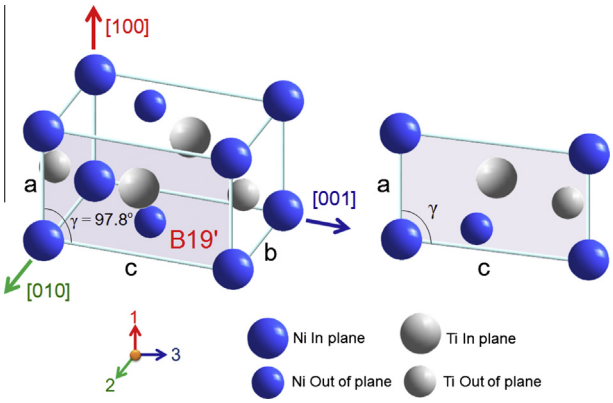


**Fig. 1.** Crystal structure of martensite B19′ NiTi. Lattice parameters *a*, *b*, and *c* and monoclinic angle $\gamma$ are marked. The blue and grey atoms represent Ni and Ti, respectively. The different size of atoms indicates atoms are in plane and out of plane. The Cartesian 1- and 2-directions are along with lattice vectors *a* and *b*. (For interpretation of the references to color in this figure legend, the reader is referred to the web version of this article.)

Yet, a clear comparison of the 13 moduli terms between martensite 'single crystals' and 'internally twinned' martensite is desired and can be obtained from 'ab initio' studies. This paper addresses this need. In particular, the shear modulus determination on the (001) twin plane is of utmost significance, it will be shown in this study that its magnitude is four times smaller for 'internally twinned' states compared to the 'single' crystal states.

The elastic moduli of martensite can be determined experimentally either below the martensite finish temperature, or during pseudoelasticity upon austenite to martensite transformation. In both cases, the elastic loading or unloading of the stress–strain curves has been extensively utilized in past studies. In the first case, the measured modulus in the martensitic regime under small (initial) deformations was found to be rather low (<50 GPa, also reported later in the paper). This led to many reports where elastic modulus of martensite was tabulated at a lower value than austenite (Hodgson et al., 1990; Duerig et al., 1990). On the other hand, the modulus of martensite after transformation or martensite deformed to high strains has been measured as rather high (>100 GPa), in fact higher than austenite modulus (Sehitoglu et al., 2000). The question then arises, what is the source of this difference?

We offer a simple explanation on this perplexing evolution in 'stress-induced' martensite elastic moduli. We use the term 'stress-induced' because of the evolving magnitude of the elastic moduli as the martensite detwins. When the SMA is cooled below martensite finish temperature under zero external stress, a self-accommodating martensite morphology develops (Otsuka and Wayman, 1998). This martensite morphology is internally twinned (Wechsler et al., 1953) and is referred to as 'thermal martensite'. When deformed in the martensitic regime, the stress–strain response is governed by the growth of preferred variants with respect to others (Duerig et al., 1990). An effective or apparent moduli, representing the detwinning of the variants, are measured. Specifically, when deformed to large strains in tension, the martensite elastic modulus will ultimately represent the displacement of atoms in '*c*' direction which is the largest lattice constant (see Fig. 1). This means that under tension loading the martensite with the longest lattice axis (termed [001] in this study) vertical is preferred. Upon application of compression, the preferred direction is [100] with the shortest lattice axis or the '*a*' axis being vertical. So, the effective modulus observed depends on the orientation (texture) of the crystal, and can exhibit tension–compression asymmetry.

The DFT (density functional theory) calculations for elastic moduli along lattice vectors should agree with the loading–unloading measurements after high strains in tension and compression. We show experimental results that conform to the statement above on laboratory samples without grain boundaries. On the other hand, these DFT calculations for single crystals cannot be directly used to establish the macroscopic moduli of the twinned structure (the initial moduli of the martensite). This paper forwards a 'twinned' crystal unit cell for modeling the twinned martensite moduli. So what should one use in mechanics (continuum or crystal level) simulations of the martensite response? To assign a constant value for martensite modulus would be deficient. This is borne out by experiment. We conduct DFT calculations and illustrate how the modulus of a 'twinned structure' can be calculated and subsequently obtain the macroscopic moduli. Also, as stated earlier we reveal a direct comparison between the shear moduli calculation based on the 'twinned state' compliance tensor and the shearing moduli from the Generalized Planar Fault Energy (GPFE) curve with very good agreement.

## 2. Elastic constants of B19′ NiTi

The martensitic NiTi has a B19′ monoclinic crystal structure with lattice parameters $a$ = 2.88 Å, $b$ = 4.11 Å, $c$ = 4.66 Å and a monoclinic angle $\gamma$ = 97.8° (Fig. 1). These parameters, determined from structural energy minimization in our previous DFT calculations (Ezaz et al., 2011), will be used in the present study. Here, the monoclinic angle $\gamma$ is between the [100] and [001] directions. The *c*-axis is the longest axis and the *a*-axis is the shortest one, while the *b*-axis is the intermediate (we

note that this notation of lattice vectors is different to the ones of Hatcher (Hatcher et al., 2009) and Wagner (Wagner and Windl, 2008), where *a*-axis is the longest axis and *c*-axis is the shortest one). In the present study, the notation of coordinate system is chosen as the Cartesian 1- and 2-directions are along with lattice vectors *a* and *b* (see Fig. 1).

A general linear stress–strain relation at constant temperature has the form:

$$\sigma_{ij} = C_{ijkl}\varepsilon_{kl}, \quad (i,j,k,l = 1,2,3) \tag{1}$$

where $\sigma_{ij}$ is a second-order stress tensor, $\varepsilon_{kl}$ is a second-order strain tensor, and $C_{ijkl}$ is a fourth-order tensor called elastic constant tensor.

The stress–strain relation is invertible as:

$$\varepsilon_{ij} = S_{ijkl}\sigma_{kl} \tag{2}$$

where $S_{ijkl}$ is a fourth-order elastic compliance tensor.

Using the Voigt's notation, the double indices can be replaced with a single indice ($11 \to 1; 22 \to 2; 33 \to 3; 23 \to 4; 13 \to 5; 12 \to 6$). Then the second-order stress tensor can be expressed with a vector as $\sigma = (\sigma_1, \sigma_2, \sigma_3, \sigma_4, \sigma_5, \sigma_6)$, and the second-order strain tensor can be written as $\varepsilon = (\varepsilon_1, \varepsilon_2, \varepsilon_3, \varepsilon_4, \varepsilon_5, \varepsilon_6)$. Similarly, the fourth-order elastic constant tensor can be reduced to a symmetric $6 \times 6$ matrix as $C_{ij}$. Therefore, the stress–strain relation can be written as:

$$\sigma_i = C_{ij}\varepsilon_j, \quad (i,j = 1,2,3,4,5,6) \tag{3}$$

**Table 1**
The calculated elastic constants for single crystal (SC) and twinned structure (TS) of martensitic B19′ NiTi are compared to Hatcher and Wagner's work.

| Elastic constants (GPa) | DFT calculations | | | |
|---|---|---|---|---|
| | Single crystal (SC) | | | Twinned structure (TS) |
| | Hatcher (Hatcher et al., 2009) | Wagner (Wagner and Windl, 2008) | This study (SC) | This study (TS) |
| $C_{11}$ | 212 | 200 | 209 | 141 |
| $C_{12}$ | 125 | 125 | 114 | 74 |
| $C_{13}$ | 99 | 99 | 102 | 102 |
| $C_{15}$ | −1 | 4 | 1 | −43 |
| $C_{22}$ | 245 | 241 | 234 | 179 |
| $C_{23}$ | 129 | 129 | 139 | 121 |
| $C_{25}$ | −3 | −9 | −7 | −24 |
| $C_{33}$ | 249 | 223 | 238 | 184 |
| $C_{35}$ | 15 | 27 | 27 | −1 |
| $C_{44}$ | 87 | 76 | 77 | 50 |
| $C_{46}$ | −4 | −4 | −5 | 1.5 |
| $C_{55}$ | 66 | 21 | 23 | 30 |
| $C_{66}$ | 86 | 77 | 72 | 67 |

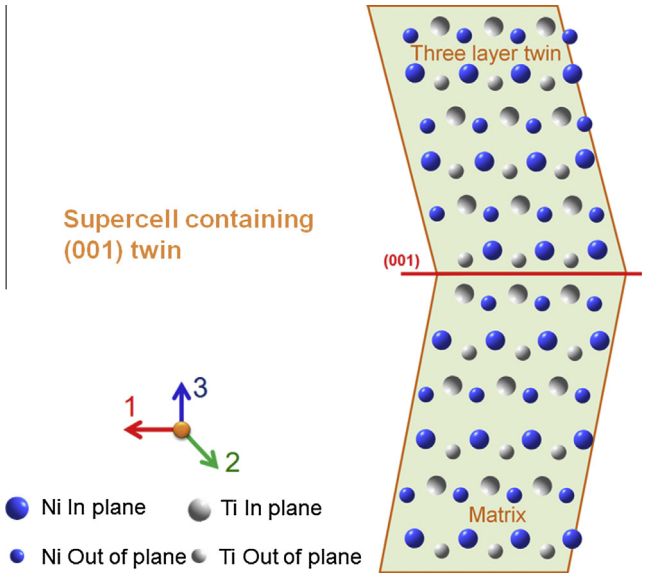


**Fig. 2.** Supercell of twinned structure B19′ NiTi containing (001) compound twin. The (001) compound twin is shown in a red line. (For interpretation of the references to color in this figure legend, the reader is referred to the web version of this article.)

**Table 2**
The compliance constants for martensitic B19′ NiTi are calculated by taking the inverse of the elastic constants matrix in Table 1.

| Compliance constants ($10^{-3}$ GPa$^{-1}$) | Single crystal (SC) | | | Twinned structure (TS) |
|---|---|---|---|---|
| | Hatcher (SC) | Wagner (SC) | This study (SC) | This study (TS) |
| $S_{11}$ | 7 | 7.8 | 6.8 | 65 |
| $S_{12}$ | −2.9 | −3.3 | −2.3 | 21 |
| $S_{13}$ | −1.3 | −1.4 | −1.7 | −49 |
| $S_{15}$ | 0.3 | −1.1 | 1 | 109 |
| $S_{22}$ | 6.9 | 9 | 8.8 | 19.3 |
| $S_{23}$ | −2.5 | −5.1 | −5.2 | −24.3 |
| $S_{25}$ | 0.8 | 11 | 9.2 | 45.1 |
| $S_{33}$ | 5.9 | 9.8 | 9.5 | 48.7 |
| $S_{35}$ | −1.5 | −14.5 | −13 | −89.2 |
| $S_{44}$ | 11.5 | 13.2 | 13 | 20 |
| $S_{46}$ | 0.5 | 0.7 | 0.9 | −0.4 |
| $S_{55}$ | 15.5 | 71.1 | 62.5 | 222.4 |
| $S_{66}$ | 11.7 | 13 | 13.9 | 14.9 |

$$\varepsilon_i = S_{ij}\sigma_j, \quad (i,j = 1,2,3,4,5,6) \tag{4}$$

Due to the symmetry of a monoclinic lattice, there are 13 independent elastic constants (compliance constants) in a monoclinic crystal structure. For the elastic constants in B19′ monoclinic NiTi, there is no reliable experimental data reported, and only theoretical calculations from DFT are available by Hatcher (Hatcher et al., 2009) and Wagner (Wagner and Windl, 2008). Due to the different notation of lattice vectors in B19′ lattice, the elastic constants shown in Table 1 are in a different order than the ones given by Hatcher and Wagner (e.g. $C_{11}$ and $C_{12}$ in Table 1 are the $C_{33}$ and $C_{32}$ in their notation). We conducted DFT simulations (utilizing the VASP code (Kresse and Furthmuller, 1996)) and determined the elastic constants for single crystal of B19′ NiTi, which are in agreement with Hatcher and Wagner.

The (001) compound twin is often experimentally observed and is energetically favored due to its small strain energy (Šesták et al., 2011; Zhao et al., 2008). Therefore, in this study we built a supercell containing (001) twin to calculate the elastic constants for the twinned structure of B19′ NiTi. Fig. 2 shows a supercell of twinned structure containing (001) compound twin. The calculated elastic constants for (001) twinned structure of B19′ NiTi are given in Table 1. We note that the (001) compound twinning mode has a significant influence on the elastic constants of B19′ NiTi, which lowers the elastic constants of the twinned structure compared to the single crystal case.

After the elastic constants are determined, the corresponding compliance constants can be calculated by taking the inverse of the elastic constants matrix. Our results for single crystal compare well to Hatcher and Wagner, and results for the twinned structure are also given in Table 2.

## 3. Shear modulus in B19′ NiTi

The shear modulus for (001)[100] twinning in B19′ NiTi can be calculated from the elastic constants (see details in Appendix A) and is expressed as following:

$$G_{(001)[100]} = \frac{1}{S_{55}} \tag{5}$$

The calculated results of 16 GPa for single crystal and 4.5 GPa for twinned structure are given in Table 3.

The twinning barriers in a crystal can be characterized by the Generalized Planar Fault Energy (GPFE) curve. The GPFE curve provides a comprehensive description of twins and is established by shearing consecutive layers along twinning direction (Kibey et al., 2007). Fig. 3 shows the GPFE curve for the (001)[100] twinning in B19′ NiTi (Ezaz et al., 2011).

A periodic supercell (no free surfaces) consisted of twelve (001) layers having four atoms per layer is created to establish the GPFE curve in B19′ NiTi. The GPFE is obtained by shearing of consecutive (001) layers starting with the twin plane along [100] direction. The process of establishing GPFE curve is shown in Fig. 4a–d. We note that unlike the cubic crystal structure,

**Table 3**
The calculated shear modulus of a single crystal and a twinned structure in B19′ NiTi is compared to Hatcher (Hatcher et al., 2009) and Wagner (Wagner and Windl, 2008).

| Twinning system | Shear modulus – theory (GPa) | | | | |
|---|---|---|---|---|---|
| | Single crystal | | | Twinned structure – this study | |
| | Hatcher | Wagner | This study | Elastic constants – Eq. (5) | GPFE Eq. (6) |
| (001)[100] | 64 | 14 | 16 | 4.5 | 4 |

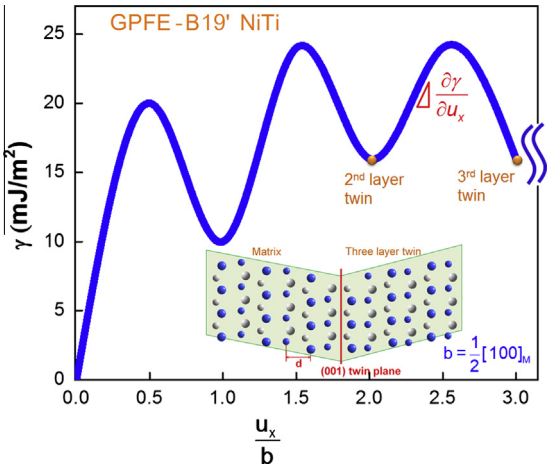


**Fig. 3.** GPFE curve for (001)[100] twinning in B19′ NiTi. This result shows that the shear modulus is 4 GPa.

to generate GPFE curve in monoclinic martensite NiTi, two (001) layers of atoms glide simultaneously with the motif points when a shear is applied in the [100] direction. As shown in Fig. 4e, the motif point is defined at the middle of each pair of Ni(Ti) atoms. Thus, the process to establish GPFE curve in B19′ NiTi with (001) twin is different to the conventional one in cubic structure (like fcc), where a consecutive single layer is sheared along twinning direction.

Fig. 4a shows a supercell consisting of nine (001) layers with (001) twin plane (red[1] line). This twin plane divides the supercell into a three-layer cell, which is fixed and forming the matrix, and a six-layer cell, which is sheared consecutively and forms the twin. The layer sequence is 1–9 from the left side to the right side of the supercell. A one-layer twin (Fig. 4b) is generated by sliding layers 4–9 relative to the fixed three-layer cell along the [100] direction through a twinning Burgers vector $b = \frac{a}{2}[100]$. A two-layer twin (Fig. 4c) is created by sliding layers 6–9 in a similar way; a three-layer twin (Fig. 4d) by sliding layers 8–9. In our GPFE calculations a full internal atom relaxation, including perpendicular and parallel directions to the twin plane, was allowed for minimizing the short-range interaction between misfitted layers. This relaxation process caused a small additional atomic displacement $r$ $\left(|r| = \sqrt{r_x^2 + r_y^2 + r_z^2}\right)$. Thus, the total fault displacement is not exactly equal to the applied shear displacement, $u$, but involves additional $r$. The GPFE calculations, involving the displacement in the parallel directions to the twin plane, provided more accurate energy barriers. Compared to the energy barrier for relaxation of only perpendicular to the twin plane, the energy barriers after full relaxation can be nearly 10% smaller.

When the GPFE is obtained from DFT calculations, we can determine the theoretical shear modulus of a twinned structure as follows (Joós et al., 1994; Kang et al., 2012; Schoeck, 2011):

$$G = \frac{2\pi d}{b}\left.\frac{\partial \gamma}{\partial u_x}\right|_{max} \tag{6}$$

where the maximum slope of GPFE curve with respect to the shear displacement is, $\left.\frac{\partial \gamma}{\partial u_x}\right|_{\max}$, $d$ is the interplanar distance and $b$ is the twinning Burgers vector. The calculated shear modulus of 4 GPa is given in Table 3.

In Table 3, we note that our calculated shear modulus for (001)[100] twinning of the single crystal B19′ NiTi is very close to Wagner's results, and it is much smaller than Hatcher's values. Most importantly, there is a significant difference between the shear modulus of a single crystal and the shear modulus of a twinned structure. We note that our calculated shear modulus for the twinned structure (4 GPa from GPFE and 4.5 GPa from elastic constants of the twinned structure) is much smaller than the one for the single crystal (16 GPa from elastic constants of the single crystal). This result indicates that B19′ NiTi twinned structure exhibits lower resistance to shear deformation compared to the single crystal case. The difference between the 4 GPa and 4.5 GPa originates from the finite number of atomic layers utilized for the GPFE calculations (<3) which is not the case in the development of the compliance tensor.

## 4. Elastic properties in B19′ NiTi

### 4.1. Elastic properties in single crystal B19′ NiTi

For B19′ monoclinic NiTi, the elastic modulus $E_{hkl}$ in a direction $l$ plane can be determined as follows (Nye, 1964; Qiu et al., 2011):

[1] For interpretation of color in 'Fig. 4', the reader is referred to the web version of this article.

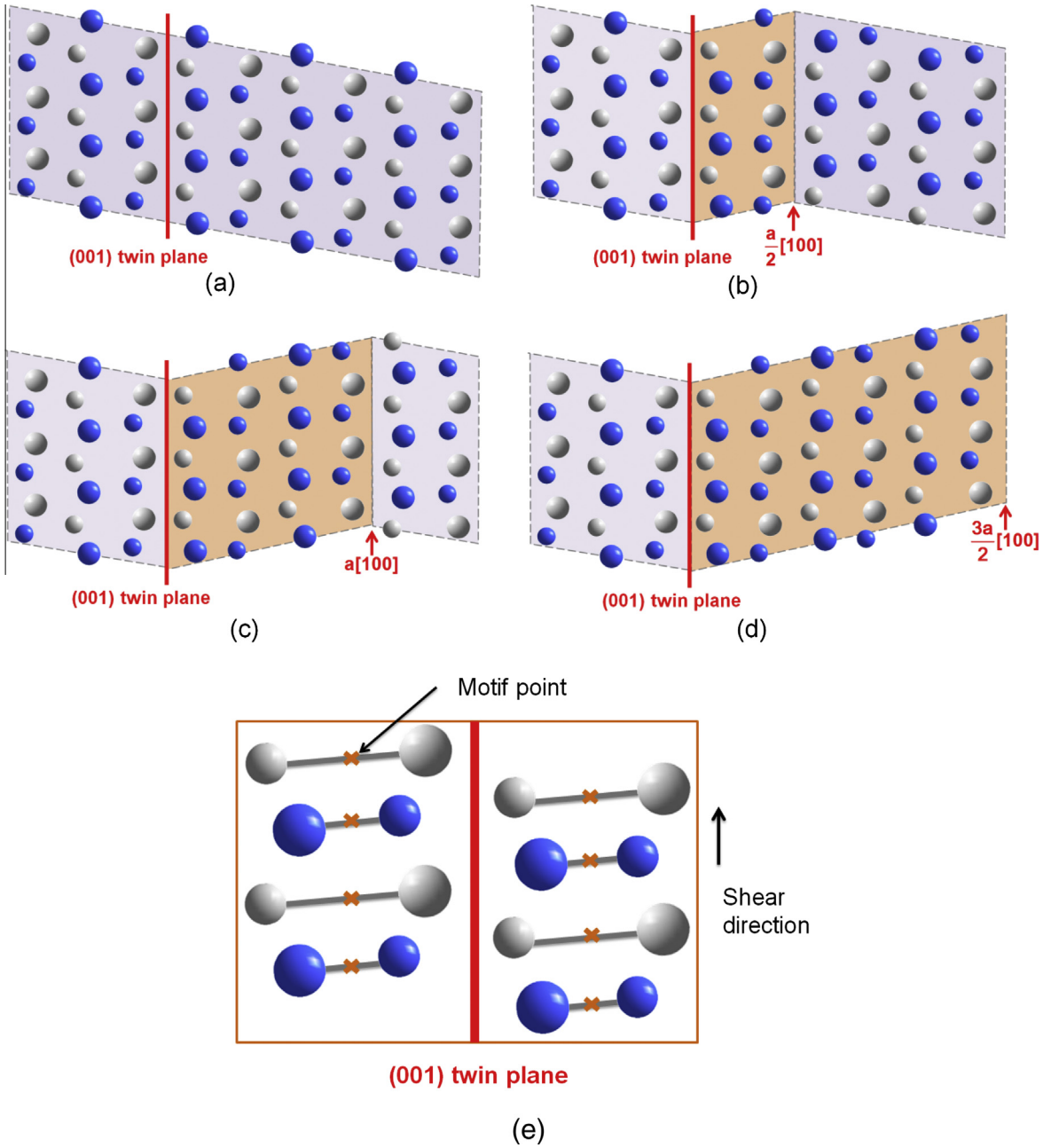


**Fig. 4.** Schematic of twin formation of B19′ NiTi in the twinning plane (0 0 1) with twinning Burgers vector $b = \frac{a}{2}[1\,0\,0]$. The view is from the [0 1 0] direction. (a) Perfect structure, (b) one-layer twin, (c) two-layer twin, (d) three-layer twin, and (e) motif points are at the middle of each pair of Ni(Ti) atoms in martensite NiTi.

$$(E_{hkl})^{-1} = n_1^4 S_{11} + 2n_1^2 n_2^2 S_{12} + 2n_1^2 n_3^2 S_{13} + 2n_1^3 n_3 S_{15} + n_2^4 S_{22} + 2n_2^2 n_3^2 S_{23} + 2n_1 n_2^2 n_3 S_{25} + n_3^4 S_{33} + 2n_1 n_3^3 S_{35} + n_2^2 n_3^2 S_{44} + 2n_1 n_2^2 n_3 S_{46} + n_1^2 n_3^2 S_{55} + n_1^2 n_2^2 S_{66} \quad (7)$$

where $n_1$, $n_2$ and $n_3$ are cosines between the direction normal to the $(h\,k\,l)$ plane and the lattice vectors ($a$, $b$ and $c$) shown in Fig. 5, $S_{ij}$ is the single crystal compliance constants given in Table 2. The elastic modulus in single crystal B19′ NiTi using Eq. (7) is calculated in Table 4. We note that there is general good agreement between the results in the present study and other calculations and experiments. The bulk modulus $B_S$ is calculated in two independent approaches (Eqs. (8) and (9)) and they yield very close results, which indicates a consistency of our calculations.

The bulk modulus $B_S$ in a single crystal is an elastic constant related to a uniform change in the atomic volume, which can be calculated from the elastic compliance constants $S$ as following (Kimizuka et al., 2008; Söderlind and Klepeis, 2009):

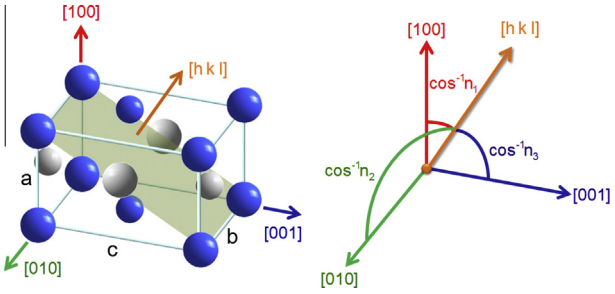


**Fig. 5.** Schematic of the angles between the direction normal to the ($hkl$) plane and the lattice vectors ($a$, $b$ and $c$).

**Table 4**
The calculated and experimental elastic modulus and bulk modulus of single crystal B19′ NiTi are compared to other DFT calculations and experiments. The single crystal results between theory and experiment by and large agree with one another.

| Elastic properties of single crystal B19′ NiTi (GPa) | DFT calculations | | | | | Experiments | |
|---|---|---|---|---|---|---|---|
| | Hatcher (Hatcher et al., 2009) | Wagner (Wagner and Windl, 2008) | Sestak (Šesták et al., 2008, 2009) | This study | | This study | Others |
| $E_{100}$ | 136 | 115 | 96 | 114 | | 107-Compression | 91 (Rajagopalan et al., 2005) |
| $E_{010}$ | 146 | 111 | 124 | 123 | | – | – |
| $E_{001}$ | 170 | 140 | 126 | 142 | | 132-Tension | 138 (Qiu et al., 2011) |
| $B_S$ | 159 | 152 | 137 | 149 Eq. (8) | 153 Eq. (9) | – | – |

$$B_S^{-1} = S_{11} + S_{22} + S_{33} + 2(S_{12} + S_{13} + S_{23}) \tag{8}$$

On the other hand, the bulk modulus $B_S$ can also be evaluated as the second derivative of total energy $U$ with respect to the unit cell volume $V$ (Gilman, 1969):

$$B_S = V\frac{d^2U}{dV^2}\bigg|_{V=V_0} \tag{9}$$

where $V_0$ = 53.68 Å$^3$ is the unconstrained unit cell volume of B19′ NiTi, and $U$ is a function of $V$ (equation of state) shown in Fig. 6. We applied hydrostatic compression pressure from 0 to 20 GPa to the unit cell of B19′ NiTi. The unit cell volume, $V$, obtained from DFT decreases continuously with increasing pressure. The insert figure of Fig. 6 shows the normalized volume compressibility curve. The structural energy, $U$, corresponding to each unit cell volume is also calculated as a function of $V$. By fitting the energy ($U$)–unit cell volume ($V$) data to a third-polynomial expression, we obtain Eq. (10):

$$U = -0.0003838V^3 + 0.0707V^2 - 4.2704V + 57 \tag{10}$$

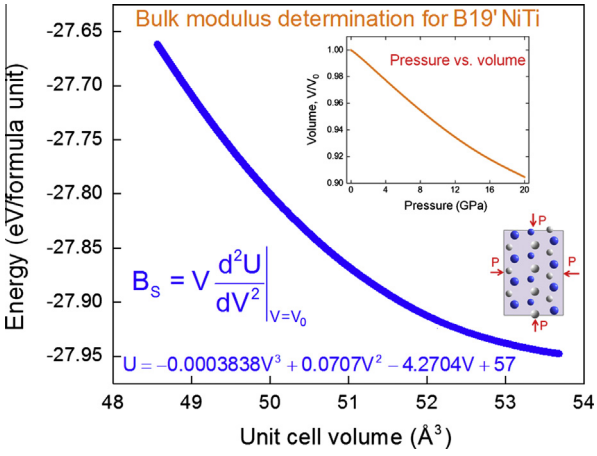


**Fig. 6.** Total energy variation with unit cell volume (applied hydrostatic pressure $P$). The bulk modulus $B_S$ is determined using Eqs. (9) and (10).

### 4.2. Elastic properties in polycrystalline B19′ NiTi

#### 4.2.1. Simulations

The macroscopic elastic modulus $E$ can be calculated by using Hill averaged values (Hill, 1952; Nye, 1964):

$$\frac{1}{E}=\frac{1}{3G}+\frac{1}{9B}$$
$$G=\frac{1}{2}(G_V+G_R),\quad B=\frac{1}{2}(B_V+B_R) \tag{11}$$

where $G_V$, $B_V$, $G_R$ and $B_R$ are Voigt (Voigt, 1928) and Reuss (Reuss and Angnew, 1929) bulk and shear moduli, which can be calculated from the elastic constants as following (Caravaca et al., 2009; Hatcher et al., 2009):

$$\begin{aligned}
15G_V &= (C_{11}+C_{22}+C_{33})-(C_{12}+C_{23}+C_{31})+3(C_{44}+C_{55}+C_{66})\\
9B_V &= (C_{11}+C_{22}+C_{33})+2(C_{12}+C_{23}+C_{31})\\
\frac{15}{G_R} &= 4(S_{11}+S_{22}+S_{33})-4(S_{12}+S_{23}+S_{31})+3(S_{44}+S_{55}+S_{66})\\
\frac{1}{B_R} &= (S_{11}+S_{22}+S_{33})+2(S_{12}+S_{23}+S_{31})
\end{aligned} \tag{12}$$

We calculated the macroscopic elastic modulus for the twinned structure of B19′ NiTi as 71 GPa, which is much smaller than the values obtained from the single crystal elastic constants by Hatcher and Wagner. Our experimental data (tension and compression tests) is also given in Table 5, and we note the results in the present study are in close agreement with experiments.

The computed macroscopic properties of B19′ NiTi are given in Table 6 and are compared to other calculations. We note that the values in single crystal are compared to Wagner's results, and the values in twinned structure are much smaller than the ones in single crystal.

#### 4.2.2. Experiments on NiTi ⟨001⟩ orientation

Fig. 7 is a schematic showing the conducted experiments to measure the elastic modulus in B19′ NiTi. All samples are single crystals with [001] orientation in the austenitic state. When NiTi is cooled below martensite finish temperature ($M_f$), a self-accommodating martensite morphology (thermal induced martensite) develops. When deformed in the martensitic regime, the initial stress–strain response reflects the elastic deformation of the self-accommodating martensite, and then the combination process of growth of preferred variant with respect to others (detwinning) and elastic deformation of the martensitic single crystal in the limit (Joós et al., 1994). The initial linear-elastic deformation is characterized by an average martensite modulus of multiple variants, $E_M^{self}$. Upon unloading the martensitic single crystal at higher strains undergoes elastic deformation with elastic modulus $E_M$, and full strain recovery is only expected upon heating above austenite finish temperature (shape memory strain is recovered). The $E_M$ should be measured in the unloading segment of the stress–strain response and as the detwinning proceeds should give a good indication of the single crystal moduli (Sehitoglu et al., 2000).

**Table 5**
Macroscopic elastic modulus measured and calculated (based on Hill average) in the present study is compared to other calculations and experimental data for the multi-variant (twinned structure) case. Our predicted level of $E$ = 71GPa (twinned structure – this study) for overall elastic modulus is consistent with the experiments. Based on single crystal constants the levels are in the range 122–180 GPa.

| Macroscopic elastic properties of twinned structure (Hill average) of B19′ NiTi (GPa) | Theory – DFT calculations | | | | Experiments | | |
|---|---|---|---|---|---|---|---|
| | Hatcher (Hatcher et al., 2009) | Wagner (Wagner and Windl, 2008) | This study | | This study | | Others (TS) |
| | | | Single crystal (SC) constants – Table 2 | Twinned structure (TS) constants – Table 2 | Tension (TS) | Compression (TS) | |
| $E$ (Eq. (11)) | 180 | 122 | 126 | 71 | 50–70 | 50–70 | 40–70 References Benafan et al. (2012), Hodgson et al. (1990), Liu and Xiang (1998), Liu and Yang (1999), Qiu et al. (2011), Rajagopalan et al. (2005), Stebner et al. (2013), and Young et al. (2010) |

**Table 6**
Macroscopic elastic properties determined in the present study utilizing SC and TS constants are compared with others in the literature.

| Macroscopic elastic properties of B19′ NiTi (GPa) | Theory – DFT calculations | | | |
|---|---|---|---|---|
| | Hatcher (Hatcher et al., 2009) | Wagner (Wagner and Windl, 2008) | This study | |
| | | | Single crystal (SC) | Twinned structure (TS) |
| $E$ | 180 | 122 | 126 | 71 |
| $G$ | 69 | 45 | 47 | 26 |
| $B$ | 158 | 147 | 152 | 79 |
| $E_V$ | 184 | 149 | 150 | 115 |
| $E_R$ | 176 | 95 | 102 | 27 |
| $G_V$ | 71 | 56 | 56 | 43 |
| $G_R$ | 67 | 34 | 37 | 10 |
| $B_V$ | 159 | 152 | 154 | 122 |
| $B_R$ | 157 | 143 | 149 | 36 |
| $\nu$ | 0.31 | 0.36 | 0.36 | 0.35 |

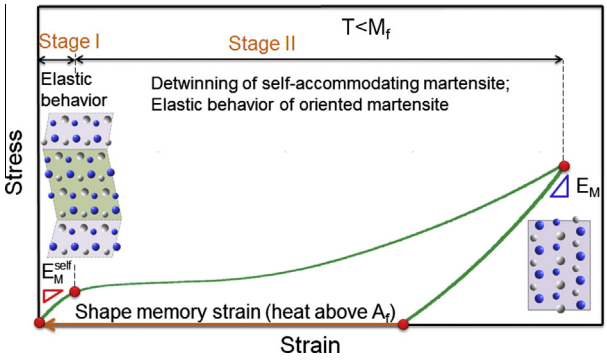


**Fig. 7.** Schematic showing the experiments conducted to measure the elastic modulus in B19′ NiTi. The twinned structure (thermal induced martensite) corresponds to $E_M^{self}$, and $E_M$ is the detwinned structure (stress induced martensite) elastic modulus.

Fig. 8 shows the elastic modulus of B19′ NiTi calculated at 0 K and measured at finite temperature (below martensite finish temperature) by Sehitoglu's group (Sehitoglu et al., 2001, 2000). The experiments were conducted under tension and compression on single crystal specimens which have an original [001] orientation in the austenitic state. We note that the experimental results reflect three states of the martensite: self-accommodating, single crystal in compression and single

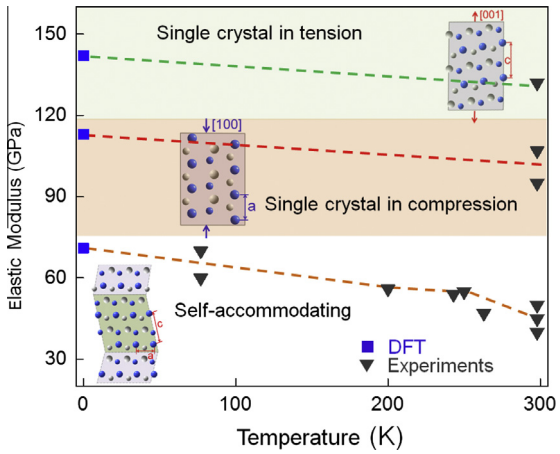


**Fig. 8.** The elastic modulus of B19′ NiTi calculated at 0 K in DFT (blue square) and measured at finite temperatures below martensite finish temperature (black triangle) by Sehitoglu's group (includes unpublished results) (Sehitoglu et al., 2001; Sehitoglu et al., 2000). The materials have three test states: self-accommodating, single crystal in compression ('*a*' vertical) and single crystal in tension ('*c*' vertical). The self-accommodating refers to 'thermal-induced' and the single crystal corresponds to 'stress-induced' martensite. (For interpretation of the references to color in this figure legend, the reader is referred to the web version of this article.)

crystal in tension. All experiments were conducted at $T \ll M_f$. The elastic moduli are determined from elastic portion of the curves at small strains (self-accommodating case) and at higher strains upon unloading (tension or compression moduli). The experiments were conducted in the temperature range 77–300 K on with nickel rich Ni (at.)–Ti alloys including the 50.1%Ni–Ti alloy which is fully martensitic below room temperature (Wagoner Johnson et al., 2005). We note that when the material is deformed to high strains, slip of martensite can occur with concomitant inelastic strains. However, the measured unloading elastic modulus methodology remains valid.

## 5. Discussion of results

In this paper, we provide a critical assessment of the elastic moduli determination based on atomistic simulations. The contribution of the paper is to present a modified unit cell which we referred to as the 'twinned state' to predict the macroscopic moduli of the internally twinned martensite. Since the macroscopic state of the material lies between the oriented (single) crystals versus the twinned state case in the limit, we point to the omnipresence of evolving elastic moduli. Therefore, we refer to the elastic moduli as 'deformation-mediated'. Specifically, our simulations are compared to macroscopic experiments for the multi-variant (twinned) and single (oriented) crystal martensites with very good agreement. We observe that the published moduli based on oriented (single crystal) martensites cannot predict the macroscopic moduli of the twinned martensite.

We note that the present results (elastic properties of single crystal B19′ NiTi in Tables 4 and 5) are in good agreement with available experimental data. The difference between the present results and Hatcher's results in Table 1 is due to the methodological difference. In the present study a full internal atom relaxation is allowed for each applied strain (lattice distortion). The total energy of the deformed crystal was minimized during this relaxation process which circumvents atoms coming too close to each other. While, in Hatcher's calculations the relaxation was not allowed for each lattice distortion, which induces a larger total energy. In Table 4, we note that the elastic modulus and bulk modulus calculated by Hatcher is larger than other DFT simulations. The consistency between our results and experiments ensures the efficacy of our calculations. Additionally, we calculated the shear modulus of twinned structure, which is much smaller than the one of single crystal (Table 3). This indicates that the shear modulus should be properly applied in mechanics simulations due to the different values between twinned structure and single crystal. However, Wagner et al. obtained the results for single crystal only and the different shear modulus of B19′ NiTi is not notified in their calculations. Furthermore, we note that the elastic constant $C_{22}$ in our calculations is smaller than $C_{33}$, but larger than $C_{11}$. This trend is consistent with Hatcher's results. However, the $C_{22}$ is the largest compared to $C_{33}$ and $C_{11}$ in Wagner's calculation results. This large discrepancy between this set of elastic constants causes different derived elastic modulus. In Table 4 we note that the elastic modulus $E_{010}$ (corresponding to the intermediate lattice parameter $b$ of B19′ NiTi) in Wagner's calculations is much smaller than ours and other DFT results, and it is even smaller than $E_{100}$ (corresponding to the smallest lattice parameter $a$ of B19′ NiTi). While, in our calculations $E_{010}$ is larger than $E_{100}$, which is consistent with other DFT calculations (Hatcher et al., 2009; Šesták et al., 2008, 2009). Thus, our calculated elastic constants are in better agreement with experiments.

The results in Fig. 8 highlight the dramatic differences between macroscopic elastic modulus (lower curve) in the twinned state (multi variant martensite) versus in the single crystal state (after detwinning) in tension (highest curve) and compression (intermediate curve). As also noted in Fig. A2 of Appendix A, the predicted elastic moduli in single crystal (SC) state in tension is higher compared to compression. Also, the SC moduli are higher than the internally twinned state (TS) moduli (Tables 4 and 5). An immediate ramification of these results is that during the course of the deformation the increase in elastic moduli of the martensite results in an increase in the elastic stored energy which opposes the transformation (Olson and Cohen, 1975). The increase in moduli necessitates further cooling under stress or increase in stress at constant temperature for completion of the transformation (Gall and Sehitoglu, 1999; Hamilton et al., 2004; Patoor et al., 1995). Therefore, the knowledge of elastic moduli levels is vital in understanding the transformation behavior and potential development of new shape memory alloys.

We draw particular attention to the prevailing shear modulus that governs the martensite deformation. The shear moduli on the (001) system is calculated as 4.5 GPa based on atomistic simulations of the TS unit cell. This shear moduli determination is in agreement with GPFE (Generalized Planar Fault Energy) calculations which is 4 GPa. On the other hand, the shear moduli calculation based on using the SC compliance tensor is four times higher (16 GPa). This is further evidence that special care must be devoted to the establishment of the 'operating' shear moduli for the detwinning of the martensite (Wang and Sehitoglu, 2013).

In the present work, we considered the twinned state of NiTi crystals as governed by the (001) twin system. An alternative twin system with a stepped interface (transformation twin or Type II-1 twin) on (111) planes is derived from the phenomenological theory of martensite transformations (Ezaz and Sehitoglu, 2011a; Xie and Yong, 2004). It is possible to establish a modified set of elastic constants for the internally twinned Type II-1 case, but in our view the (001) case illustrates our point, and is more prevalent particularly in aged NiTi alloys (Gall et al., 1999a,b). The wide range of twin systems have been discussed by Ishida and colleagues (Zhang et al., 2006), and analyzed by Sehitoglu and colleagues (Ezaz and Sehitoglu, 2011b; Wang and Sehitoglu, 2013).

We note that in the case of NiTi alloys, the NiTi compositions near 50.1% Ni exhibit transformation temperatures near room temperature while higher Ni contents (such as >51.5%Ni) result in transformation temperatures well below 77 K

(Johnson et al., 2005). Therefore to determine the 'twinned state' macroscopic moduli, it is desirable to choose the Ni compositions and test temperatures in experiments judiciously ($T \ll M_f$). To determine single crystal properties, it is best to deform martensite to high strains at $T \ll M_f$. If martensite moduli is determined from the unloading curve after austenite to martensite transformation at $T > A_f$, care must be taken that the slope is not influenced by the reversed transformation or back stress effects. All the experimental results (for $T \ll M_f$ case) are combined in Fig. 8 and compared to simulations from ab initio calculations and Hill's estimate. We note that the dramatic difference in measured elastic moduli at 300 K: from self-accommodated martensite (45 GPa) to single crystal martensite upon tension (130 GPa) and upon compression (100 GPa). These experimental results validate the simulations (albeit at 0 K) also marked in Fig. 8.

It is worthwhile to highlight the importance of having accurate martensite moduli for fracture and fatigue studies in shape memory alloys. For example, in fracture mechanics, the crack tip displacement fields are a strong function of elastic modulus. To calibrate fracture or fatigue models errors in elastic moduli can lead to errors in the determination of energy release rates upon crack advance. The toughening in phase transformation is known to be affected by the elastic moduli (McMeeking and Evans, 1982). Any attempts to understand the driving forces in shape memory alloys, particularly for stress-induced or thermal induced martensites (Brinson, 1993), necessitates correct description for the governing moduli (Gall and Sehitoglu, 1999). Similarly, when analyzing the fatigue response and the calculations of elastic and plastic strain portions of hysteresis loops (Gall et al., 2001; Melton and Mercier, 1979), one must also have the correct elastic moduli values. In fact, the phenomenological models as well as micro-mechanical models rely on the decomposition of the strain to elastic and plastic portions. In this regard, one should note the asymmetry of tension and compression elastic moduli in the modeling efforts.

The knowledge of the correct moduli is also valuable in the assessment of the strength levels (slip resistance) in NiTi martensitic crystals and also composite behavior of austenite–martensite domains during thermo-elastic deformation. In the presence of precipitates, the strengthening is affected by the resistance to slip, in the form of Orowan strengthening, which is directly proportional to the shear modulus. Also, in the presence of austenite and martensite domains, the ensemble deformation behavior is affected by the moduli of the individual phases. This is particularly important in phenomenological models. Also, during fatigue deformation the presence of residual martensites alters the mechanical response. The residual martensites can represent sources of internal stress whose magnitude scales with the elastic moduli and affect the response cycle after cycle. In addition, the elastic moduli evolution influences the hardening response, which undergoes complicated transients in the case of fatigue of shape memory alloys (Gall et al., 2001).

We draw attention to the difference in the theoretical results for single crystal martensite among the three studies summarized in this study. The atomistic code used by Wagner and the current work is the same (VASP). On the other hand, the atomistic code used by Hatcher and Sestak differ. It is insightful to note that the overall elastic moduli predicted by the four studies (for single crystal) are comparable (Table 4) while the shear moduli, such as on (001) planes, differ (Table 3). Since the shear modulus for the (001) plane is rather low, this is the plane where deformation twinning occurs (Wang and Sehitoglu, 2013). Hence, the determination of modulus for this plane is extremely relevant.

The presence of internally twinned martensites as studied above has close resemblance to the modulated structures that are prevalent in the monoclinic phases of a number of new shape memory alloys. The low elastic moduli in the martensitic state is characteristic of the Heusler alloys such as NiMnGa and NiFeGa (Wang et al., 2014). In the case of such alloys the elastic moduli is also dictated by the presence of modulations reminiscent of internal twin boundaries.

The paper focused on the elastic constants in the martensitic phase. We note that the elastic constants for the austenitic phase are well established in the literature, and there is agreement among the different works on its magnitude (Hatcher et al., 2009; Wagner and Windl, 2008). Three elastic constants for the cubic crystal (single crystal state) have been reported in numerous publications and also have been experimentally determined (Benafan et al., 2013; Ren et al., 2001; Sehitoglu et al., 2002). The combined knowledge of austenite and martensite moduli will provide the basis for simulation of shape memory and pseudoelastic behavior.

## 6. Conclusions

The work supports the following conclusions:

(1) The work underscores the importance of determining the elastic moduli for the internally twinned crystal structure. This improves the understanding of the macroscopic martensite moduli of 'twinned martensite' observed in experiments. The viewing of the elastic moduli with 3D plots illustrates the anisotropy of the 'twinned' state constants which are lower than the 'detwinned' single crystal constants.

(2) The experimental observation of low elastic modulus at the macroscopic level in the twinned state in NiTi agrees with the theoretical results. Moreover, the results are in close agreement when shear moduli on the (001) twin plane is determined by two methods: the derivative of the Generalized Planar Fault Energy curves and the elastic moduli coefficients determined by application of prescribed strain tensors to the unit cell in the twinned state.

(3) A number of mesoscale mechanics formulations have been developed in the literature to predict pseudoelasticity and shape memory relying on the evolution of austenite and martensite phase volume fractions. In these formulations either the moduli of austenite and martensite are assumed to be the same, or the austenite modulus is assumed to

be higher. We note that there is a need to better characterize the martensite elastic moduli evolution upon conversion from 'thermal-induced' to 'stress-induced' martensite as the detwinning-induced microstructural arrangements are responsible for the measured elastic moduli. The calculations utilizing DFT pointed to the higher moduli values for martensite in the 'single crystal' state, and lower macroscopic values for martensite in the 'internally twinned' state.

## Acknowledgements

The support of the work by National Science Foundation, CMMI 13-33884, is gratefully acknowledged. We also acknowledge the use of the Taub cluster provided by the Computational Science and Engineering Program at the University of Illinois.

## Appendix A. Elastic constants determination of monoclinic crystal structure

The unstrained crystal lattice of B19′ NiTi is defined by the lattice vectors **a**, **b** and **c** with length $a = 2.88$ Å, $b = 4.11$ Å, $c = 4.66$ Å and a monoclinic angle $\gamma = 97.8°$. Utilizing DFT simulations, we can calculate the total energy for arbitrary crystal structures (strained crystals), which are obtained when small (initial) strain is applied to the unstrained lattice. The lattice vectors **a**′, **b**′ and **c**′ for an arbitrary crystal structure can be determined according to the following rule (Ravindran et al., 1998; Wagner and Windl, 2008). This transformation is referred to as the Cauchy–Born rule (Ericksen, 2008).

$$(\mathbf{a}', \mathbf{b}\prime, \mathbf{c}\prime) = (\mathbf{a}, \mathbf{b}, \mathbf{c}) \cdot D \tag{A1}$$

where $D$ is called distortion matrix containing the strain component, $\varepsilon$, and (**a**, **b**, **c**) denotes the undeformed lattice. The distortion matrix is chosen as volume conserving ($\det D = 1$) to obtain the shear constants, while $\det D = 1 + \varepsilon$ (non volume conserving) to obtain the other elastic constants. For each applied strain magnitude, a corresponding distortion matrix is obtained, and thus lattice vectors of the strained crystal can be determined in Eq. (A1). The total energy for the strained crystal, $U(V, \varepsilon)$, associated with each set of lattice vectors or distortion matrix (applied strain), can then be calculated from DFT.

The total energy for an arbitrary crystal structure (strained crystal), $U(V, \varepsilon)$, can be expanded in Taylor series in powers of the strain tensor with respect to the total energy for the unstrained crystal as (Ravindran et al., 1998; Söderlind and Klepeis, 2009):

$$U(V, \varepsilon) = U(V_0, 0) + V_0\left(\sum_i \tau_i \xi_i \varepsilon_i + \frac{1}{2}\sum_{ij} C_{ij}\varepsilon_i\xi_i\varepsilon_j\xi_j\right) + O(\varepsilon^3) \tag{A2}$$

where $U(V, \varepsilon)$ and $U(V_0, 0)$ are the total energies corresponding to the strained and unstrained crystals, respectively; $V$ is the volume of the strained crystal, and $V_0$ is the volume of the unstrained crystal. The $C_{ij}$ represents the elastic constants in the Voigt notation described earlier. Essentially, the difference $U(V, \varepsilon) - U(V_0, 0)$ involves the change in energy due to applied strain. These values are computed from the DFT calculations. In Eq. (A2), the Voigt notation has been used, so *xx*, *yy*, *zz*, *yz*, *xz* and *xy* are replaced by 1, 2, 3, 4, 5 and 6. $\xi_i$ is a factor considering the difference between the Cauchy's shear strain and engineering shear strains, and equals to 1 for $i = 1$, 2, 3 and 2 for $i = 4$, 5 and 6. $\tau_i$ is a component of the stress tensor. In practice, the higher-order term $O(\varepsilon^3)$ is neglected and this equation can be written in quadratic form as:

$$U(V, \varepsilon) = U(V_0, 0) + V_0(\tau\varepsilon + \frac{1}{2}C\varepsilon^2) \tag{A3}$$

where $\tau$ is introduced as a linear combination of stress components and $C$ represents a linear combination of elastic constants. The elastic constants can be deduced as proportional to the second order coefficient in a polynomial fit of the total energy as a function of the strain. Since there are 13 independent elastic constants in a monoclinic structure, 13 different distortion matrices $D$ are needed to compute the different total energies $U(V, \varepsilon)$, and the corresponding elastic coefficients $C$ in Eq. (A3) can thus be derived.

We demonstrate how to compute the elastic constant $C_{33}$ in the twinned structure B19′ NiTi. We applied very small magnitude of strain $\varepsilon$ ($-0.02$, $-0.01$, 0.01 and 0.02) in the present study to minimize the errors from higher order terms in Eq. (A2). The distortion matrix $D_3$ to calculate $C_{33}$ is defined as follows:

$$D_3 = \begin{pmatrix} 1 & 0 & 0 \\ 0 & 1 & 0 \\ 0 & 0 & 1+\varepsilon \end{pmatrix} \tag{A4}$$

where $\varepsilon = -0.02$, $-0.01$, 0.01, 0.02, and four corresponding $D_3$ are then defined.

By substituting the four $D_3$ into Eq. (A1), we can determine lattice vectors for four strained crystals. Note that when $\varepsilon = 0$, the $D_3$ is a unit matrix and the lattice vectors represent the unstrained crystal. From DFT simulations, we can calculate the total energy $U(V, \varepsilon)$ associated with these strained and unstrained crystals. These energy values corresponding to $\varepsilon$ are shown as black squares in Fig. A1. The black curve is a second order polynomial function to fit these values and has the formula as follows (note that the energy unit is eV, and $1\ \text{eV} = 1.6 \times 10^{-19}$ J):

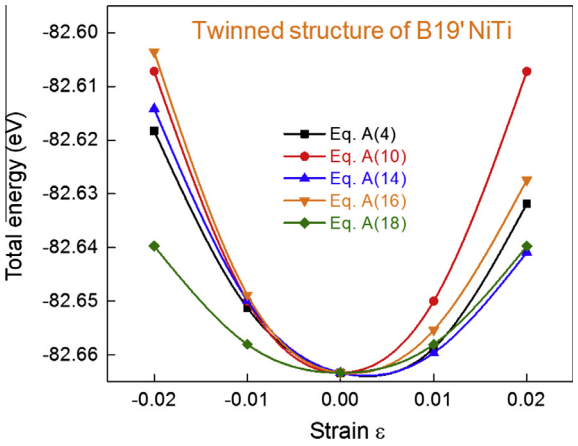


**Fig. A1.** The total energy $U(V, \varepsilon)$ associated with $D$ as a function of strain $\varepsilon$ for the twinned structure B19′ NiTi. The points represent the calculated values and the curves are the second order polynomial fit.

$$U(\varepsilon) = -82.66 - 0.346\varepsilon + 97\varepsilon^2 \tag{A5}$$

In Fig. A1, we also show calculated energies and their corresponding polynomial fit curves associated with several distortion matrices, which are defined later. These energy values and fit functions are used to compute the elastic constants.

On the other hand, the total energy $U(V, \varepsilon)$ associated with $D_3$ in Eqs. (A2) and (A3) can be written as follows ($\xi_i = 1$, $C = C_{33}$ and $\tau_3$ is the corresponding stress component):

$$U(V, \varepsilon) = U(V_0, 0) + V_0\left(\tau_3\varepsilon + \frac{C_{33}}{2}\varepsilon^2\right) \tag{A6}$$

where $U(V_0, 0) = -82.66$ eV, and $V_0 = 167.9$ Å$^3$ $= 167.9 \times 10^{-30}$ m$^3$.

Since Eqs. (A5) and (A6) represent the same $U(V, \varepsilon)$ for certain $\varepsilon$, we can calculate the elastic constant $C_{33} = 184$ GPa from the following equation (the energy unit, eV, in Eq. (A5) is converted into $J$ by multiplication of $1.6 \times 10^{-19}$):

$$\frac{C_{33}}{2} \times 167.9 \times 10^{-30} = 97 \times 1.6 \times 10^{-19} \tag{A7}$$

Similarly, all elastic constants can be calculated. The distortion matrices $D$ and elastic coefficients $C$ used in the present study are defined as follows.

The distortion matrix $D$ can be expressed as the summation of a unit matrix $I$ and 9 base matrices $H_{rs}$ with $r, s = 1, 2, 3$ (the $(r; s)$ entry of $H_{rs}$ is 1 and the other entries are zero). Thus, $D_3$ in Eq. (A4) can be expressed as $D_3 = I + \varepsilon H_{33}$, and other 12 distortion matrices can be written as:

$$D_1 = I + \varepsilon H_{11}, \quad C = C_{11} \tag{A8}$$

$$D_2 = I + \varepsilon H_{22}, \quad C = C_{22} \tag{A9}$$

$$D_4 = \frac{I + \varepsilon(H_{23} + H_{32})}{1 - \varepsilon^2}, \quad C = 4C_{44} \tag{A10}$$

$$D_5 = \frac{I + \varepsilon(H_{13} + H_{31})}{1 - \varepsilon^2}, \quad C = 4C_{55} \tag{A11}$$

$$D_6 = \frac{I + \varepsilon(H_{12} + H_{21})}{1 - \varepsilon^2}, \quad C = 4C_{66} \tag{A12}$$

$$D_7 = \frac{I + \varepsilon(H_{11} - H_{22})}{1 - \varepsilon^2}, \quad C = C_{11} + C_{22} - 2C_{12} \tag{A13}$$

$$D_8 = \frac{I + \varepsilon(H_{11} - H_{33})}{1 - \varepsilon^2}, \quad C = C_{11} + C_{33} - 2C_{13} \tag{A14}$$

$$D_9 = \frac{I + \varepsilon(H_{22} - H_{33})}{1 - \varepsilon^2}, \quad C = C_{22} + C_{33} - 2C_{23} \tag{A15}$$

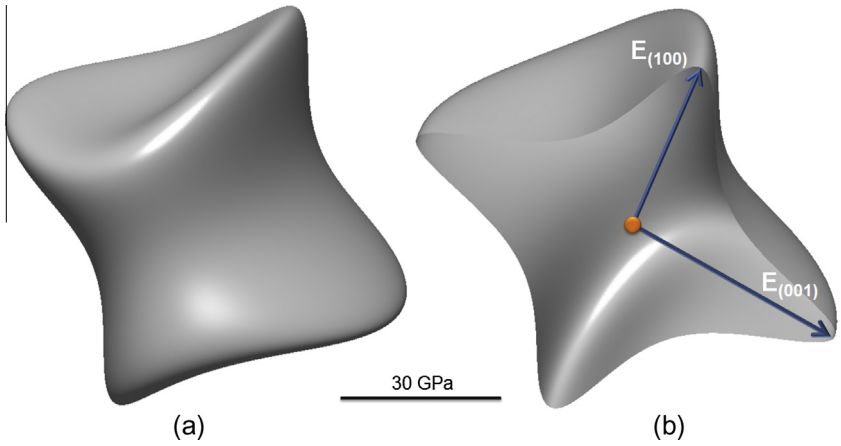


**Fig. A2.** (a) Representation surface of direction-dependent elastic moduli for twinned structure B19′ NiTi. (b) The middle cut view of the representation surface. The length of the radius vector in the normal direction of $(hkl)$ plane is defined as the elastic modulus $E_{hkl}$ in Eq. (7). The numerical results are given in Table 5.

$$D_{10} = \frac{I + \varepsilon(H_{11} + H_{13} - H_{23})}{1 - \varepsilon^2}, \quad C = C_{11} + C_{22} + C_{55} - 2(C_{12} - C_{15} + C_{25}) \tag{A16}$$

$$D_{11} = \frac{I + \varepsilon(H_{11} + H_{13} - H_{33})}{1 - \varepsilon^2}, \quad C = C_{11} + C_{33} + C_{55} - 2(C_{13} - C_{15} + C_{35}) \tag{A17}$$

$$D_{12} = I + \varepsilon(H_{12} + H_{23}), \quad C = C_{44} + C_{66} + C_{55} \tag{A18}$$

$$D_{13} = \frac{I + \varepsilon(H_{11} + H_{13})}{(1 + \varepsilon)}, \quad C = C_{11} + C_{55} + 2C_{15} \tag{A19}$$

The calculated elastic constants for twinned structure B19′ NiTi are given in Table 1, and the corresponding compliance constants are calculated in Table 2. By substituting the compliance constants into Eq. (7), the elastic modulus $E_{hkl}$ along normal direction of arbitrary $(hkl)$ planes can be computed (Ericksen, 2008; Wagner and Windl, 2008). The representation surface of direction-dependent elastic moduli for twinned structure B19′ NiTi is shown in Fig. A2, where the length of the radius vector in the normal direction of $(hkl)$ plane is defined as $E_{hkl}$.

## References


Auricchio, F., Taylor, R.L., Lubliner, J., 1997. Shape-memory alloys: macromodelling and numerical simulations of the superelastic behavior. Comput. Methods Appl. Mech. Eng. 146, 281–312.

Benafan, O., Noebe, R., Padula II, S., Gaydosh, D., Lerch, B., Garg, A., Bigelow, G., An, K., Vaidyanathan, R., 2012. Temperature dependent behavior of a polycrystalline NiTi shape memory alloy around the transformation regime. Scr. Mater. 68, 571–574.

Benafan, O., Noebe, R.D., Padula Ii, S.A., Garg, A., Clausen, B., Vogel, S., Vaidyanathan, R., 2013. Temperature dependent deformation of the B2 austenite phase of a NiTi shape memory alloy. Int. J. Plast. 51, 103–121.

Brinson, L.C., 1993. One-dimensional constitutive behavior of shape memory alloys: thermomechanical derivation with non-constant material functions and redefined martensite internal variable. J. Intell. Mater. Syst. Struct. 4, 229–242.

Caravaca, M., Mino, J., Pérez, V., Casali, R., Ponce, C., 2009. Ab initio study of the elastic properties of single and polycrystal $TiO_2$, $ZrO_2$ and $HfO_2$ in the cotunnite structure. J. Phys.: Condens. Matter 21, 015501.

Ericksen, J.L., 2008. On the Cauchy–Born rule. Math. Mech. Solids 13, 199–220.

Ezaz, T., Sehitoglu, H., 2011a. Coupled shear and shuffle modes during twin growth in B2-NiTi. Appl. Phys. Lett. 98, 241906.

Ezaz, T., Sehitoglu, H., 2011b. Type II detwinning in NiTi. Appl. Phys. Lett. 98.

Ezaz, T., Sehitoglu, H., Maier, H.J., 2011. Energetics of twinning in martensitic NiTi. Acta Mater. 59, 5893–5904.

Funakubo, H., 1987. Shape Memory Alloys. Gordon and Breach Science Publishers (translated from the Japanese by J.B. Kennedy).

Gall, K., Sehitoglu, H., 1999. The role of texture in tension–compression asymmetry in polycrystalline NiTi. Int. J. Plast. 15, 69.

Gall, K., Sehitoglu, H., Anderson, R., Karaman, I., Chumlyakov, Y.I., Kireeva, I.V., 2001. On the mechanical behavior of single crystal NiTi shape memory alloys and related polycrystalline phenomenon. In: Micromechanics and Micromechanisms of Deformation and Fracture: In Honor of Professor Ali S. Argon, 1999, first–second ed. Elsevier, Switzerland, pp. 85–92.

Gall, K., Sehitoglu, H., Chumlyakov, Y.I., Kireeva, I.V., 1999a. Tension–compression asymmetry of the stress–strain response in aged single crystal and polycrystalline NiTi. Acta Mater. 47, 1203–1217.

Gall, K., Sehitoglu, H., Chumlyakov, Y.I., Kireeva, I.V., Maier, H.J., 1999b. The influence of aging on critical transformation stress levels and martensite start temperatures in NiTi. I. Aged microstructure and micro-mechanical modeling. Trans. ASME J. Eng. Mater. Technol. 121, 19–27.

Gilman, J.J., 1969. Micromechanics of Flow in Solids. McGraw-Hill.

Hamilton, R.F., Sehitoglu, H., Chumlyakov, Y., Maier, H.J., 2004. Stress dependence of the hysteresis in single crystal NiTi alloys. Acta Mater. 52, 3383.

Hatcher, N., Kontsevoi, O.Y., Freeman, A.J., 2009. Role of elastic and shear stabilities in the martensitic transformation path of NiTi. Phys. Rev. B (Condens. Matter Mater. Phys.) 80, 144203, 144218pp.

Hill, R., 1952. Proc. Phys. Soc 65, 349.
Hodgson, D.E., Ming, W., Biermann, R.J., 1990. Shape memory alloys, . 10th ed. Metals Handbook 10th ed., vol. 2 ASM International, pp. 897–902.
Johnson, A.J.W., Hamilton, R.F., Sehitoglu, H., Biallas, G., Maier, H.J., Chumlyakov, Y.I., Woo, H.S., 2005. Analysis of multistep transformations in single-crystal NiTi. Metall. Mater. Trans. A 36, 919.
Joós, B., Ren, Q., Duesbery, M.S., 1994. Peierls–Nabarro model of dislocations in silicon with generalized stacking-fault restoring forces. Phys. Rev. B 50, 5890–5898.
Kang, K., Bulatov, V.V., Cai, W., 2012. Singular orientations and faceted motion of dislocations in body-centered cubic crystals. Proc. Natl. Acad. Sci. 109, 15174–15178.
Kibey, S., Liu, J.B., Johnson, D.D., Sehitoglu, H., 2007. Predicting twinning stress in fcc metals: linking twin-energy pathways to twin nucleation. Acta Mater. 55, 6843.
Kimizuka, H., Ogata, S., Li, J., 2008. Hydrostatic compression and high-pressure elastic constants of coesite silica. J. Appl. Phys. 103, 053506.
Kresse, G., Furthmuller, J., 1996. Efficient iterative schemes for ab initio total-energy calculations using a plane-wave basis set. Phys. Rev. B (Condens. Matter) 54, 11169.
Lagoudas, D.C.E., 2010. Shape Memory Alloys. Springer.
Liang, C., Rogers, C.A., 1990. One-dimensional thermomechanical constitutive relations for shape memory materials. J. Intell. Mater. Syst. Struct. 1, 207–234.
Liu, Y., Xiang, H., 1998. Apparent modulus of elasticity of near-equiatomic NiTi. J. Alloy. Compd. 270, 154–159.
Liu, Y., Xie, Z., Van Humbeeck, J., Delaey, L., 1999. Some results on the detwinning process in NiTi shape memory alloys. Scr. Mater. 41, 1273–1281.
Liu, Y., Yang, H., 1999. The concern of elasticity in stress-induced martensitic transformation in NiTi. Mater. Sci. Eng., A 260, 240–245.
McMeeking, R.M., Evans, A.G., 1982. Mechanics of transformation-toughening in brittle materials. J. Am. Ceram. Soc. 65, 242–246.
Melton, K.N., Mercier, O., 1979. Fatigue of NiTi thermoelastic martensites. Acta Metall. 27, 137–144.
Nye, F., 1964. Physical Properties of Crystals. Clarendon Press, Oxford.
Olson, G.B., Cohen, M., 1975. Thermoelastic behavior in martensitic transformations. Scr. Metall. 9, 1247.
Otsuka, K., Wayman, C.M., 1998. Shape Memory Materials. Cambridge University Press, Cambridge.
Patoor, E., Eberhardt, A., Berveiller, M., 1995. Micromechanical modelling of the superelastic behavior. J. Phys. 5, 2.
Petr Šittner, L.H., Pilch, Jan, Curfs, Caroline, Alonso, Thiery, Favier, Denis, Caroline, Alonso, Thiery, FavierCurfs, Denis, 2013. Young's modulus of austenite and martensite phases in superelastic NiTi wires. SMST Abstract, Prague, Czech Republic.
Qiu, S., Clausen, B., Padula II, S., Noebe, R., Vaidyanathan, R., 2011. On elastic moduli and elastic anisotropy in polycrystalline martensitic NiTi. Acta Mater. 59, 5055–5066.
Rajagopalan, S., Little, A., Bourke, M., Vaidyanathan, R., 2005. Elastic modulus of shape-memory NiTi from in situ neutron diffraction during macroscopic loading, instrumented indentation, and extensometry. Appl. Phys. Lett. 86, 081901.
Ravindran, P., Fast, L., Korzhavyi, P., Johansson, B., Wills, J., Eriksson, O., 1998. Density functional theory for calculation of elastic properties of orthorhombic crystals: application to $TiSi_2$. J. Appl. Phys. 84, 4891–4904.
Ren, X., Miura, N., Zhang, J., Otsuka, K., Tanaka, K., Koiwa, M., Suzuki, T., Chumlyakov, Y.I., Asai, M., 2001. A comparative study of elastic constants of Ti–Ni based alloys prior to martensitic transformation. Mater. Sci. Eng., A 312, 196–206.
Reuss, A., Angnew, Z., 1929. A calculation of the bulk modulus of polycrystalline materials. Math. Meth. 9, 55.
Schoeck, G., 2011. The Peierls stress in a simple cubic lattice. Phys. Status Solidi (B) 248, 2284–2289.
Sehitoglu, H., Hamilton, R., Canadinc, D., Zhang, X.Y., Gall, K., Karaman, I., Chumlyakov, Y., Maier, H.J., 2003. Detwinning in NiTi alloys. Metall. Mater. Trans. A 34, 5.
Sehitoglu, H., Jun, J., Zhang, X., Karaman, I., Chumlyakov, Y., Maier, H.J., Gall, K., 2001. Shape memory and pseudoelastic behavior of 51.5%Ni–Ti single crystals in solutionized and overaged state. Acta Mater. 49, 3609–3620.
Sehitoglu, H., Karaman, I., Anderson, R., Zhang, X., Gall, K., Maier, H.J., Chumlyakov, Y., 2000. Compressive response of NiTi single crystals. Acta Mater. 48, 3311–3326.
Sehitoglu, H., Zhang, X., Chumlyakov, Y., Karaman, I., Gall, K., Maier, H., 2002. Observations on stress-induced transformations in NiTi alloys. In: IUTAM Symposium on Mechanics of Martensitic Phase Transformation in Solids. Springer, pp. 103–109.
Šesták, P., Černý, M., Pokluda, J., 2008. Elastic properties of B19′ structure of NiTi alloy under uniaxial and hydrostatic loading from first principles. Strength Mater. 40, 12–15.
Šesták, P., Černý, M., Pokluda, J., 2009. Influence of comp ound twinning on Young's moduli in NiTi martensite. In: European Symposium on Martensitic Transformations. EDP Sciences, p. 06039.
Šesták, P., Černý, M., Pokluda, J., 2011. Can twinning stabilize B19′ structure in NiTi martensite? Intermetallics 19, 1567–1572.
Söderlind, P., Klepeis, J.E., 2009. First-principles elastic properties of α-Pu. Phys. Rev. B 79, 104110.
Stebner, A., Brown, D., Brinson, L., 2013. Young's modulus evolution and texture-based elastic–inelastic strain partitioning during large uniaxial deformations of monoclinic nickel–titanium. Acta Mater. 61, 1944–1956.
Duerig, T.W., Melton, K.N., Stockel, D., Wayman, C.M. (Eds.), 1990. Engineering Aspects of Shape Memory Alloys. Butterworth-Heinemann, Boston.
Tanaka, K., 1986. A thermomechanical sketch of shape memory effect: one-dimensional tensile behavior. Res. Mech. 18, 251–263.
Voigt, W., 1928. Lehrbuch der kristallphysik: (mit ausschluss der kristalloptik). BG Teubner.
Wagner, M.F.X., Windl, W., 2008. Lattice stability, elastic constants and macroscopic moduli of NiTi martensites from first principles. Acta Mater. 56, 6232.
Wagoner Johnson, A.J., Hamilton, R.F., Sehitoglu, H., Biallas, G., Maier, H.J., Chumlyakov, Y.I., Woo, H.S., 2005. Analysis of multistep transformations in single-crystal NiTi. Metall. Mater. Trans. A (Phys. Metall. Mater. Sci.) 36A, 919–928.
Wang, J., Sehitoglu, H., 2013. Twinning stress in shape memory alloys: theory and experiments. Acta Mater. 61, 6790–6801.
Wang, J., Sehitoglu, H., Maier, H.J., 2014. Dislocation slip stress prediction in shape memory alloys. Int. J. Plast. 54, 247–266.
Wechsler, M.S., Lieberman, D.S., Read, T.A., 1953. On theory of formation of martensite. J. Met. 5, 1503–1515.
Xie, Z.L., Yong, L., 2004. HRTEM study of 011 type II twin in NiTi shape memory alloy. Phil. Mag. 84, 3497–3507.
Young, M., Wagner, M.-X., Frenzel, J., Schmahl, W., Eggeler, G., 2010. Phase volume fractions and strain measurements in an ultrafine-grained NiTi shape-memory alloy during tensile loading. Acta Mater. 58, 2344–2354.
Zhang, J.X., Sato, M., Ishida, A., 2006. Deformation mechanism of martensite in Ti–rich Ti–Ni shape memory alloy thin films. Acta Mater. 54, 1185.
Zhao, J., Meng, F., Zheng, W., Li, A., Jiang, Q., 2008. Theoretical investigation of atomic-scale (0 0 1) twinned martensite in the NiTi alloy. Mater. Lett. 62, 964–966.